

Modeling rings and spirals in barred galaxies using manifolds: morphology and kinematics

M. Romero-Gómez¹, E. Athanassoula², A. Bosma², and J. J. Masdemont³

¹ Dept. d'Astronomia i Meteorologia, Institut de Ciències del Cosmos (ICC), Universitat de Barcelona (IEEC-UB), Martí i Franquès 1, E08028 Barcelona, Spain

² Laboratoire d'Astrophysique de Marseille (LAM), UMR6110, CNRS/Université de Provence, Technopôle de Marseille Etoile, 38 rue Frédéric Joliot Curie, 13388 Marseille Cédex 20, France

³ I.E.E.C & Dep. Mat. Aplicada I, Universitat Politècnica de Catalunya, Diagonal 647, 08028 Barcelona, Spain

Abstract

In a series of papers we proposed a theory to explain the formation and properties of rings and spirals in barred galaxies. The building blocks of these structures are orbits trapped by the invariant manifolds of the periodic orbits around the unstable Lagrangian points located near the ends of the bar. Here we will first present a comparison of the morphology of observed and theoretical spirals and rings. We compare the ratio of ring diameters in theory and in observations and predict that more elliptical rings will correspond to stronger forcings at and somewhat beyond corotation. We show that the shapes of observed and theoretical spirals agree and predict that stronger non-axisymmetric forcings will drive more open spirals. Secondly, we will also present the kinematics along the manifold loci, to allow comparisons with the observed kinematics along the ring and spiral loci. Finally, we consider also gaseous arms and their relations to stellar ones.

1 Introduction

This work was initially motivated by observing several images of barred galaxies of different morphologies, namely barred spirals and ringed galaxies. The outer rings in ringed galaxies are classified according the relative orientation of the semi-major axis of the ring with respect to the semi-major axis of the bar. Thus, there are three possibilities, namely R_1 ring if the two structures are perpendicular, R_2 ring if they are parallel and R_1R_2 ring if both types of rings are present. The idea of using the invariant manifolds of the periodic orbits located at the ends of the bar comes from Celestial Mechanics. Invariant manifolds associated to

periodic orbits are used in the Restricted Three Body Problem and its variations to design low-cost orbits. They are implicitly related to the transfer of matter. Here we compute the invariant manifolds in a galactic context, i.e. using a potential that describes the galaxy.

2 Short description of the manifolds and their characteristics

The equations of motion in the rotating reference frame are written in vectorial form as follows:

$$\ddot{\mathbf{r}} = -\nabla\Phi_{\text{eff}} - 2(\boldsymbol{\Omega} \times \dot{\mathbf{r}}), \quad (1)$$

where $\mathbf{r} = (x, y, z)$ is the position vector, $\boldsymbol{\Omega} = (0, 0, \Omega)$ is the rotation velocity vector around the z -axis counter-clockwise, and $\Phi_{\text{eff}} = \Phi - \frac{1}{2}\Omega^2(x^2 + y^2)$ is the effective potential. The potential Φ consists of the superposition of an axisymmetric component plus another bar-like. The Jacobi constant or energy in the rotating frame is defined as $E_J = \frac{1}{2}|\dot{\mathbf{r}}|^2 + \Phi_{\text{eff}}$. The system is static, i.e. it does not evolve in time. In this frame, the bar is fixed and located along the x -axis.

This system has five equilibrium points located in the galactic plane ($z = 0$) and where the first derivatives of the effective potential vanish. L_1 and L_2 are located along the bar's semi-major axis and are linearly unstable of the saddle type. L_3 is located in the galactic center and L_4 and L_5 along the bar's semi-minor axis. The latter are linearly stable and of the center type. Around the equilibrium points there exist families of periodic orbits. If we focus on the orbits around L_1 and L_2 , these are unstable and, thus, they cannot trap material around them, unlike the stable ones. There exist, however, other type of orbits that drive the motion. These are called the invariant manifolds. The left panel of Fig. 1 shows the motion around the equilibrium point L_1 . In white, we plot the periodic orbit of a given energy while in green and red we plot the stable and unstable branches of the invariant manifolds. Note that they remind the saddle behaviour, having two branches in the inner part of the galaxy and two in the outer part. The invariant manifolds act as flux tubes in phase space that drive the motion. The unstable branches are formed by orbits that depart from the vicinity of the periodic orbit, while the stable branches are formed by orbits that approach the periodic orbit. Thus, the invariant manifolds connect the inner parts of the galaxy with the outer parts, and vice-versa.

By varying the main parameters of the model, namely the bar pattern speed and the bar mass/strength, we obtain the different morphologies mentioned in Sect. 1 (see Fig. 2).

The variation of the pattern speed and the bar mass/strength does not result in a random shape of the invariant manifolds. In the right panel of Fig. 1 we show the 2-dimensional parameter study. On the x -axis, we decrease the bar pattern speed from left to right and on the y -axis we increase the bar mass/strength. The colour code is defined as follows: in black we plot the manifolds with a two-armed spiral; in blue, the R_2 rings; in red, the R_1R_2 rings; in orange, the R'_1 pseudorings and, in green, the R_1 rings. Note that the morphologies are not distributed randomly in the parameter space, but they are grouped in a diagonal form, i.e. at the top left corner (strong and rapidly rotating bars) we obtain spiral arms and R_2 and R_1R_2 rings, while on the bottom right corner (weak and slowly rotating bars) we obtain

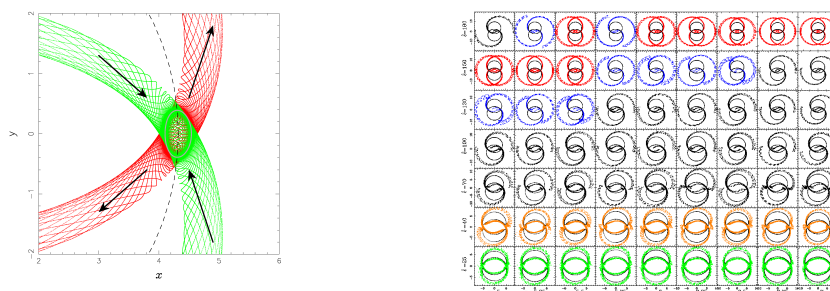


Figure 1: *Left*: Motion around the L_1 equilibrium point. In gray solid lines, we plot a periodic orbit, while in red and green we plot the unstable and stable branches of the invariant manifolds, respectively. *Right*: Two-dimensional parameter study: variation of the bar pattern speed, on the x -axis, and the bar mass/strength, on the y -axis. The colours show the different morphologies obtained (see text)

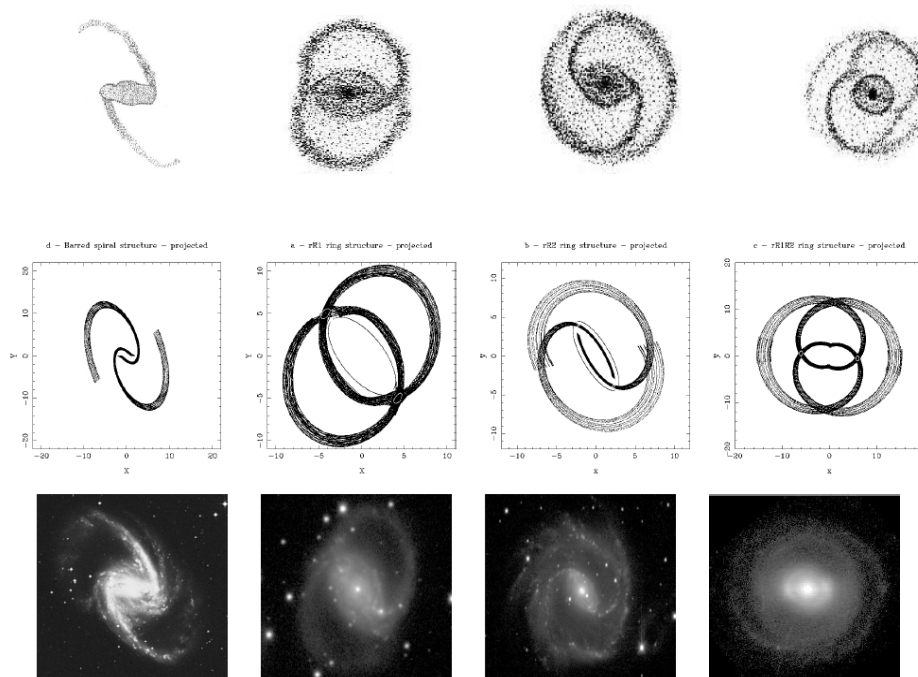


Figure 2: The four different morphologies. From left to right, the barred spiral, the R_1 ring, the R_2 ring and R_1R_2 ring.

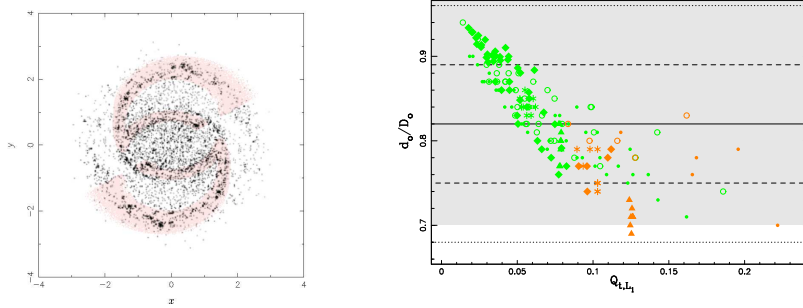


Figure 3: *Left*: The effect of the gas in the manifold orbits. Comparison with test particle simulations [1]. *Right*: Axial ratio of the outer ring as a function of the tangential force of the bar at the corotation radius.

R_1 rings and pseudorings.

Another characteristic worth mentioning is the effect of the gas in the orbits described by the manifolds. [1] uses test particle simulations to study the effect of the gas in the particles by simulating shocks of gas clouds during the integration. We perform a similar approach by reducing the kinetic energy at two random positions during the integration. The results are shown in the left panel of Fig. 3. The black dots are the results of the Schwarz's simulation while the pink lines are the manifold orbits affected by the gas.

3 Results

Here we present the results when we compare the modelled structures with observations. We compare them in two terms, first, morphologically and, second, kinematically.

3.1 Morphology

In [3] we perform several comparison with observations regarding the morphology of the models obtained. One of the comparisons is the axial ratio of the outer ring. [5] computes the axial ratio of outer R_1 rings of statistically deprojected galaxies. Here we use the same technique in order to compute the axial ratio in the modelled rings. The results are shown in the right panel of Fig. 3 where we plot the ratio as a function of the bar tangential force at corotation. The gray shaded region corresponds to the range determined by [5] for typical axial ratios, the solid line marks the mean ratio, the dashed line, the 1σ deviation and the dotted line, the 2σ deviation. The different symbols correspond to all the models computed in the paper with different bar potentials. Note that in all cases, the axial ratio of the modelled ring falls well within the observed range and the strong correlation between the axial ratio

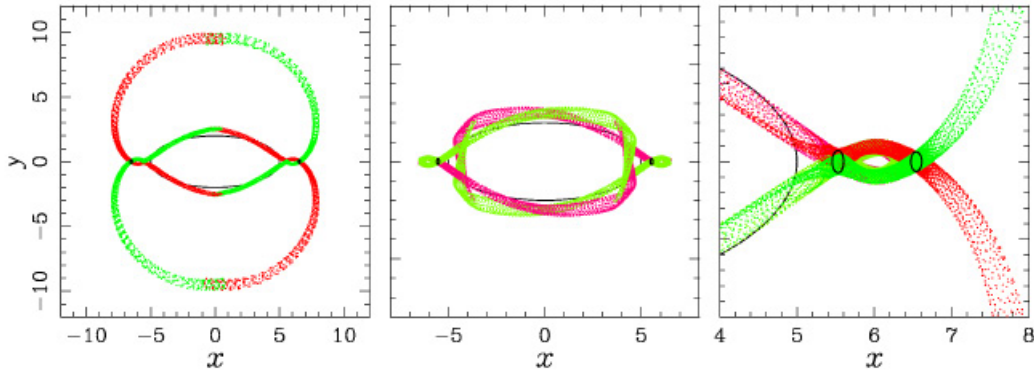


Figure 4: The invariant manifolds in the case of ansae bars. *Left*: global morphology. *Center*: inner branches delineating the rectangular shape of bars. *Right*: zoom in the region of the equilibrium points.

and the strength of the bar.

Another morphological test is to check whether the type of bar has an influence on the global morphology, that is, whether ansae bars change the morphology obtained with normal bars [2]. In this case, we simulate an ansae bar adding to the potential two small and relatively massive disks located at the ends of the bar. By changing the mass of the small disks we make the equilibrium points to bifurcate obtaining three equilibrium points, instead of one at each side of the bar. Now L_1 and L_2 become linearly stable and there appear two saddle points at both sides. The global morphology, however, does not change. See Fig. 4.

3.2 Kinematics

Here we compute the radial and tangential velocities along the manifolds in the inertial frame in two different cases, namely the R_1 ring and the spiral arms. The results are shown in the top left and top right panels of Fig. 5, respectively. Note that the amplitudes do not exceed the 20 km s^{-1} , while the radial velocities in the spiral case, do exceed the value of 50 km s^{-1} . The red line marks the mean velocity. In the bottom panels, we compute the line-of-sight velocities in each case for different viewing angles, namely 0° , 30° , 45° , 90° , 135° , and 180° . The red line here is the fitting to a sine curve. Note that in the ring case we obtain a good match to the fitting, while the kinematics of the spiral arms seem that they cannot be fitted to a sine curve, meaning that a sinusoidal curve cannot be used to determine the galaxy major axis [4].

Acknowledgments

This work is partially supported by grant ANR-06-BLAN-0172 and by the Spanish MICINN - FEDER grant AYA2009-14648-C02-01 and CONSOLIDER CSD2007-00050.

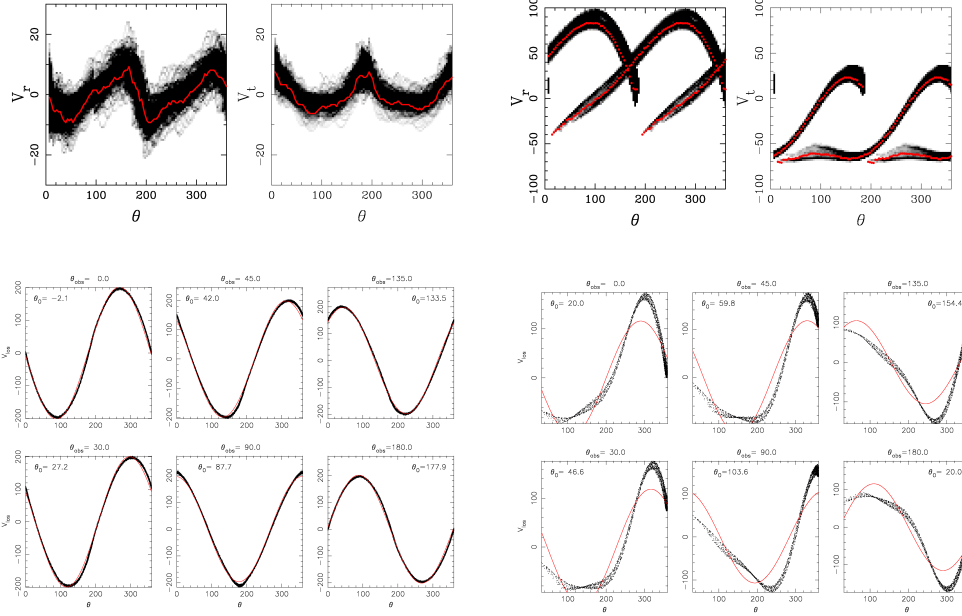


Figure 5: Kinematics. *Left*: kinematics of the R_1 ring. *Right*: kinematics of the spiral arms. *Top panels*: radial and tangential velocities in the inertial frame along the manifolds. *Bottom panels*: line-of-sight velocities at different viewing angles.

References

- [1] Schwarz, M. P. 1984, MNRAS, 209, 93
- [2] Athanassoula, E., Romero-Gómez, M., & Masdemont, J. J. 2009a, MNRAS, 394, 67
- [3] Athanassoula, E., Romero-Gómez, M., Bosma, A., & Masdemont, J. J. 2009b, MNRAS, 400, 1706
- [4] Athanassoula, E., Romero-Gómez, M., Bosma, A., & Masdemont, J. J. 2010, MNRAS, 407, 1433
- [5] Buta, R. 1995, ApJS, 96, 39